

Resolving the tropical Pacific/Atlantic interaction conundrum

Feng Jiang¹, Wenjun Zhang^{1*}, Fei-Fei Jin², Malte F. Stuecker³, Axel Timmermann^{4,5},
Michael J. McPhaden⁶, Julien Boucharel^{2,7}, and Andrew T. Wittenberg⁸

¹ Key Laboratory of Meteorological Disaster of Ministry of Education (KLME), Nanjing University of Information Science and Technology, Nanjing, China.

² Department of Atmospheric Sciences, School of Ocean and Earth Science and Technology (SOEST), University of Hawai'i at Mānoa, Honolulu, HI, USA.

³ Department of Oceanography & International Pacific Research Center (IPRC), School of Ocean and Earth Science and Technology (SOEST), University of Hawai'i at Mānoa, Honolulu, HI, USA.

⁴ Institute for Basic Science, Center for Climate Physics, Busan, South Korea.

⁵ Pusan National University, Busan, South Korea.

⁶ NOAA/Pacific Marine Environmental Laboratory, Seattle, Washington.

⁷ CNRS/LEGOS, 14 avenue Edouard Belin, 31400, Toulouse, France.

⁸ National Oceanic and Atmospheric Administration/Geophysical Fluid Dynamics Laboratory, Princeton, New Jersey.

Contents of this file

Texts S1 to S2

Figures S1 to S9

Tables S1 to S3

Introduction

This supporting information provides detailed explanation about the established ENSO-forced recharge oscillator model for Atlantic Niño, details about the targeted pacemaker experiments, and figures/tables supplementary to the main text.

Text S1.

To confirm the different responses of equatorial Atlantic variability to ENSO events with different evolution features, we conducted two sets of sensitivity experiments (EXP_early and EXP_late) using the Geophysical Fluid Dynamics Laboratory Global Coupled Model version 2.1 (Delworth et al., 2006). The resolution of the atmospheric component is $2^\circ \times 2.5^\circ$ with 24 vertical levels, and the resolution of the oceanic component is 1° in the extratropics with meridional spacing decreasing to $1/3^\circ$ near the equator.

In the first set of experiments (EXP_early), the time-evolving SST anomalies of observed early-onset ENSO events were added to the seasonally-varying climatological SST in the tropical Pacific region (20°S – 20°N , 160°E – 100°W), which were calculated as half the difference between composite early-onset El Niño and early-onset La Niña. Similarly, the time-evolving SST anomalies of observed late-onset ENSO were prescribed in the second set of experiments (EXP_late). Here the observed early-onset and late-onset types of ENSO events are selected based on the ± 0.5 standard deviation of the Niño3.4 index in early spring to summer (April to June). The early-onset El Niño events are 1982, 1987, 1997, 2002, 2009, 2015, 2019; the early-onset La Niña events are 1984, 1995, 1988, 1999; the late-onset El Niño events are 1986, 1991, 1994, 2006, 2018; and the late-onset La Niña events are 1983, 1998, 2005, 2007, 2010, 2011, 2016, 2017. The time-evolving SST anomalies were then added to the seasonally varying climatological SST from January to December. The SSTs were allowed to evolve freely outside of the prescribed regions. These two sets of experiments both consist of an ensemble of 10 simulations, and the ensemble mean was analyzed. Considering the large common bias for current models to simulate climatological features, especially in the equatorial Atlantic region, we here focus on the difference between these two sets of experiments.

Text S2.

An extended version of the original recharge oscillator (RO) model (Jin, 1997; Stuecker et al., 2017) is considered for the Atlantic Niño (Eq. 1-2) that incorporates background state modulated remote ENSO forcing:

$$\frac{dT_a}{dt} = RT_a + \gamma h_a + \alpha T_E, \quad (1)$$

$$\frac{dh_a}{dt} = \varepsilon h_a + \lambda T_a + \beta T_E, \quad (2)$$

where the background state modulation is taken as a first-order approximation, that is, only the annual cycle is taken into consideration (Eq. 3-8):

$$R = R_0 + R_a \cos(\omega_a t + \varphi_{R_a}), \quad (3)$$

$$\gamma = \gamma_0 + \gamma_a \cos(\omega_a t + \varphi_{\gamma_a}), \quad (4)$$

$$\varepsilon = \varepsilon_0 + \varepsilon_a \cos(\omega_a t + \varphi_{\varepsilon_a}), \quad (5)$$

$$\lambda = \lambda_0 + \lambda_a \cos(\omega_a t + \varphi_{\lambda_a}), \quad (6)$$

$$\alpha = \alpha_0 + \alpha_a \cos(\omega_a t + \varphi_{\alpha_a}), \quad (7)$$

$$\beta = \beta_0 + \beta_a \cos(\omega_a t + \varphi_{\beta_a}). \quad (8)$$

The model parameters were estimated using multiple linear regression that minimizes the root-mean-square error in 1-month forecasts based on monthly values of Atlantic Niño SST anomalies (T_a , Atl3 index), equatorial Atlantic thermocline depth (h_a , averaged over 3°S–3°N, 70°W–20°E) and ENSO SST anomaly forcing (T_E , Niño3.4 index). Here the depth of 20 °C isotherm is used as an estimate of the thermocline. Detailed information and estimated values are given in Table S3.

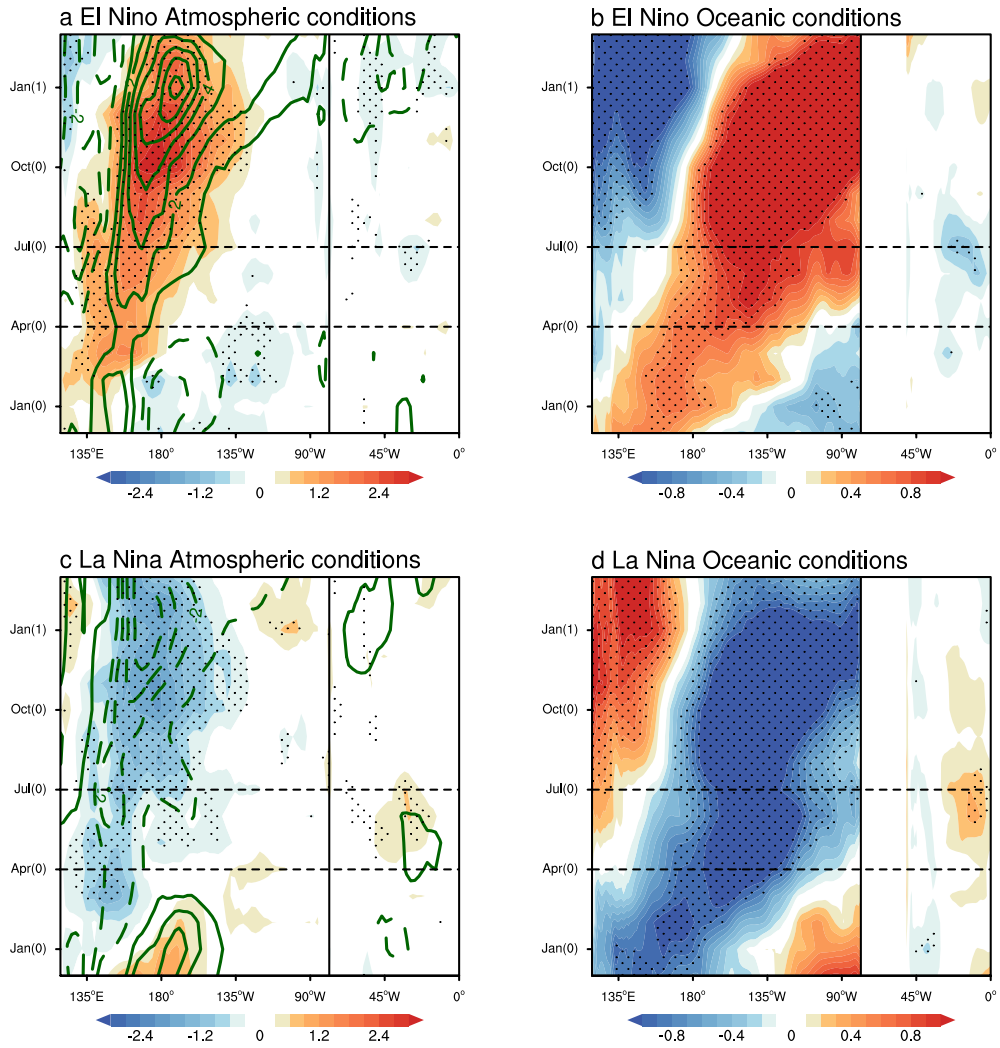


Figure S1. Similar to Figure 2 (c) and (d) but for El Niño and La Niña events separately.

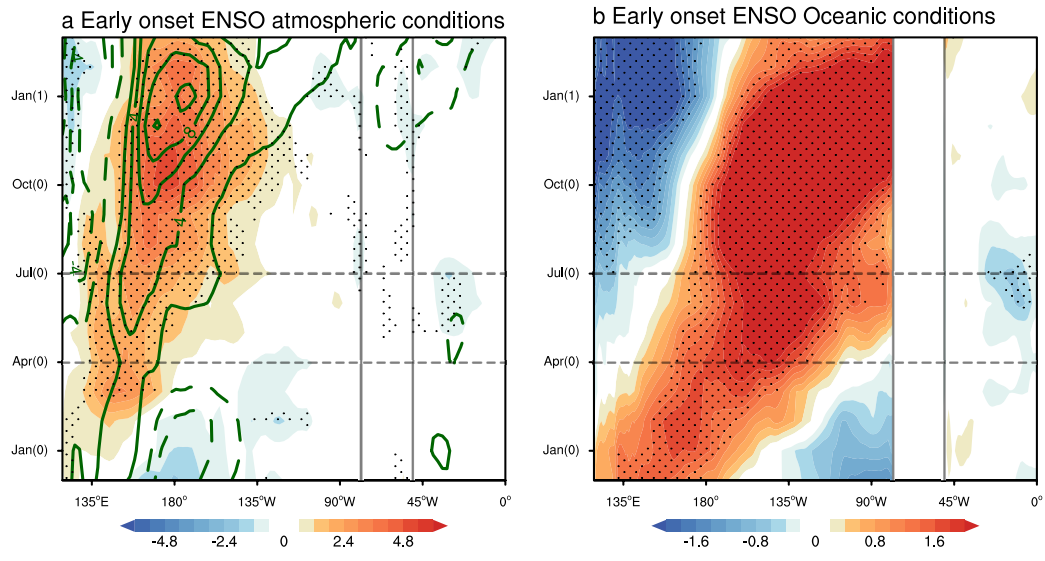


Figure S2. Similar to Figure 2 (c) and (d) but for early-onset ENSO events.

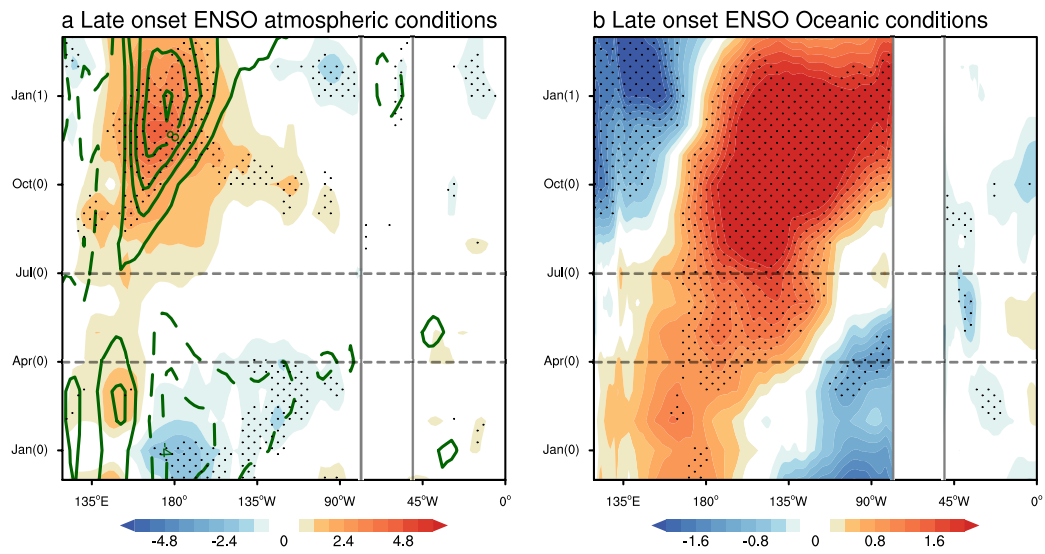


Figure S3. Similar to Figure 2 (c) and (d) but for late-onset ENSO events.

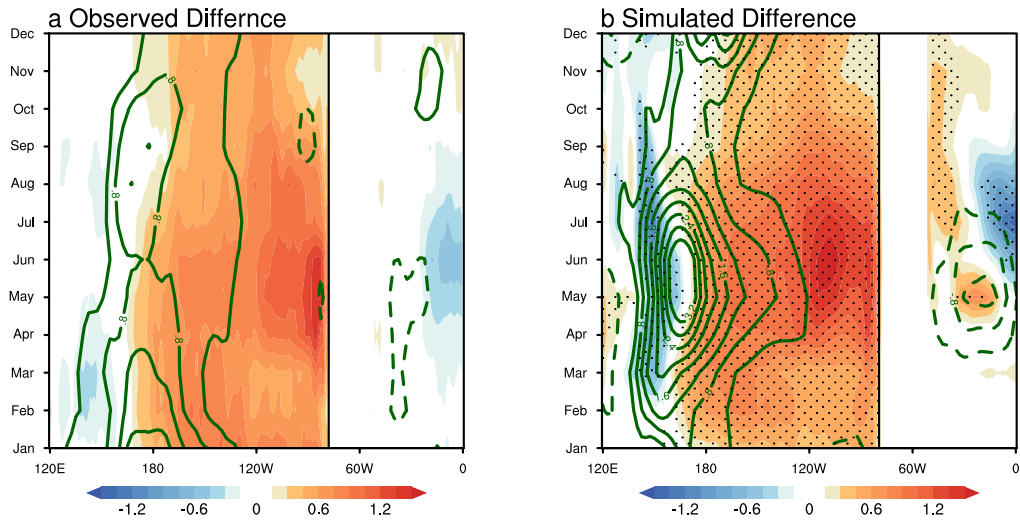


Figure S4. (a) Hovmöller diagrams for the temporal evolution of SST anomalies (shading; °C) and surface zonal wind anomalies (contour; m/s) for the difference early-onset ENSO (half the difference between El Niño and La Niña) and late-onset ENSO events in the observations. The contour interval is 0.4 m/s and the zero value is omitted. (b) Similar to (a) but for the difference between the ensemble-mean of EXP_early and that of EXP_late. Dots in (b) indicate the difference of SST anomalies between the two ensembles is statistically significant at the 95% confidence level.

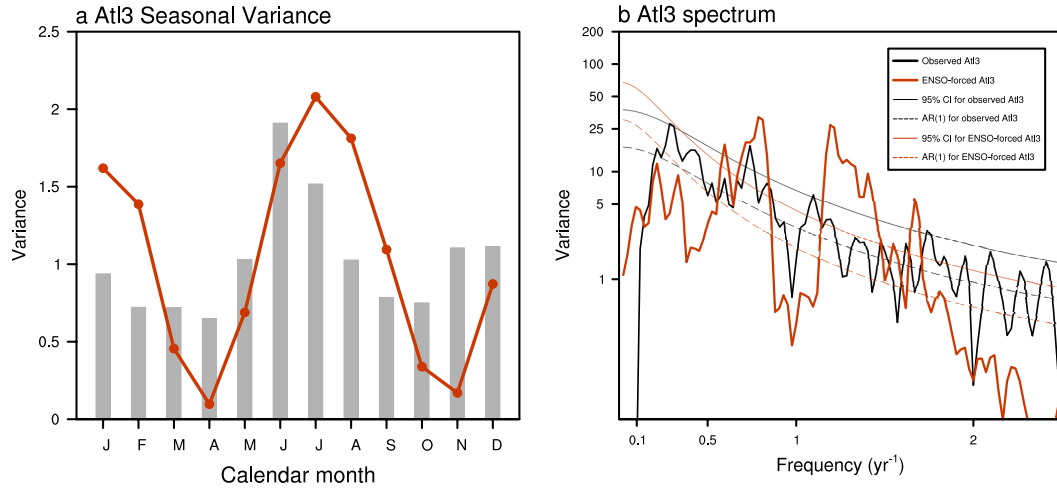


Figure S5 (a) Seasonal variance of the standardized observed AtI3 index (gray bar) with standardized ENSO-forced RO AtI3 index (red line). **(b)** Spectra for observed (thick black line) and ENSO-forced RO AtI3 index (thick red line). The AR(1) null hypothesis is displayed by a dashed thin line and the 95% confidence level is indicated by a solid thin line for observed (black) and ENSO-forced RO AtI3 index (red) respectively.

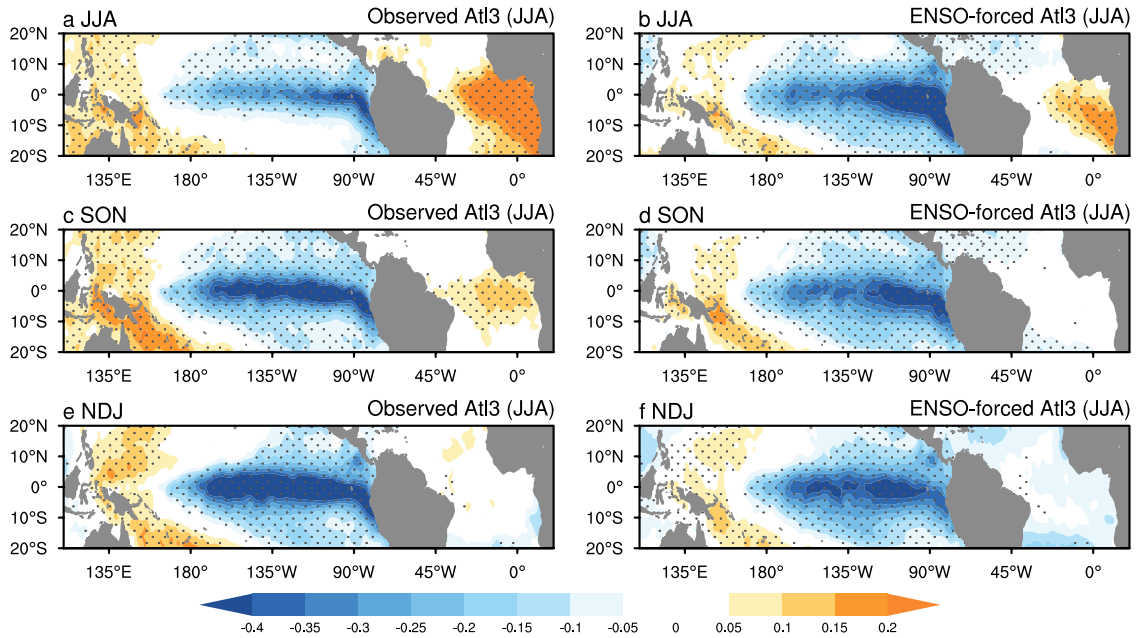


Figure S6. (a) Boreal summer (June to August, JJA), (c) autumn (September to November, SON) and (e) winter (November to January, NDJ) SST anomalies (shading; °C) regressed on the observed previous summer (JJA) AtI3 index. The right panels (b, d and f) are similar to the left panels but for the ENSO-forced RO AtI3 index. Dots indicate values that are statistically significant at the 95% confidence level.

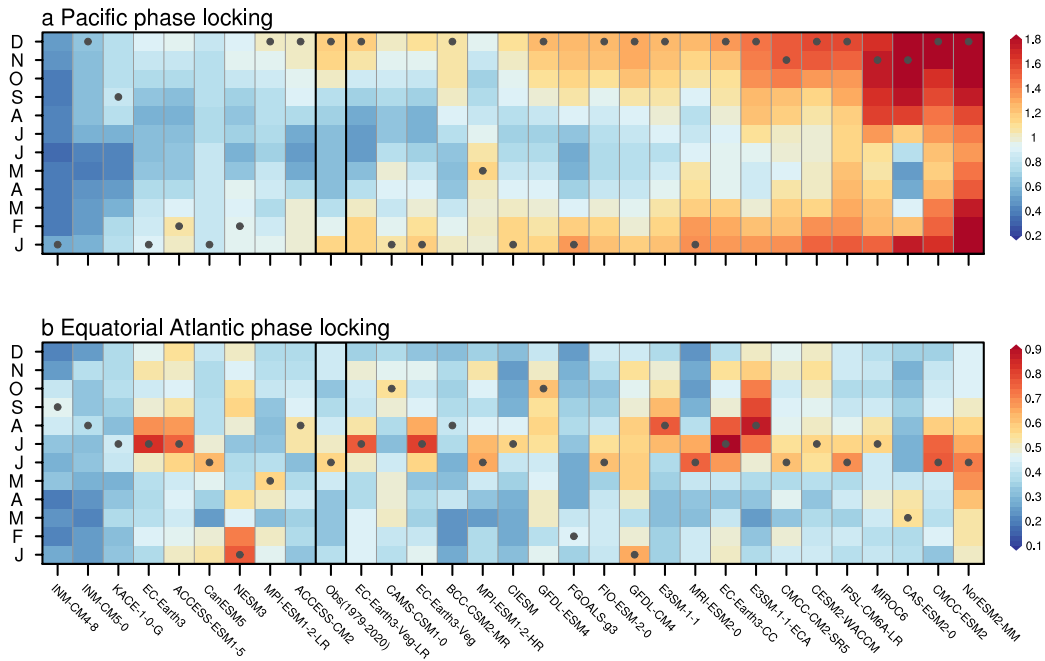


Figure S7. (a) Standard deviation of the Niño3.4 index stratified by calendar month for CMIP6 extended historical simulations, sorted by the strength of the annual mean standard deviation in an ascending order. The black dots indicate the calendar month with the maximum standard deviation for each model and the observations. The observations are shown for reference. **(b)** Similar to **(a)** but for the Atl3 index.

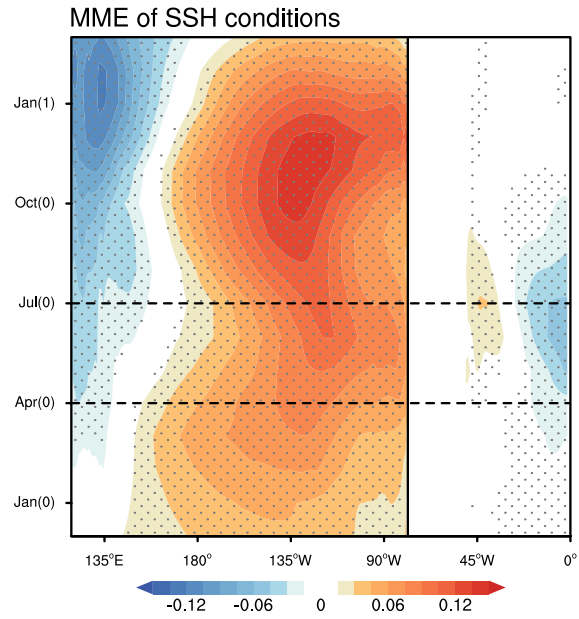


Figure S8. Hovmöller diagram for the multi-model ensemble (MME) mean temporal evolution of sea surface height (SSH; shading; cm) for ENSO years with opposite-signed summer equatorial Atlantic events (El Niño minus La Niña) in 20 CMIP6 extended historical simulations. Dots indicate SSH anomalies that are statistically significant at the 95% confidence level.

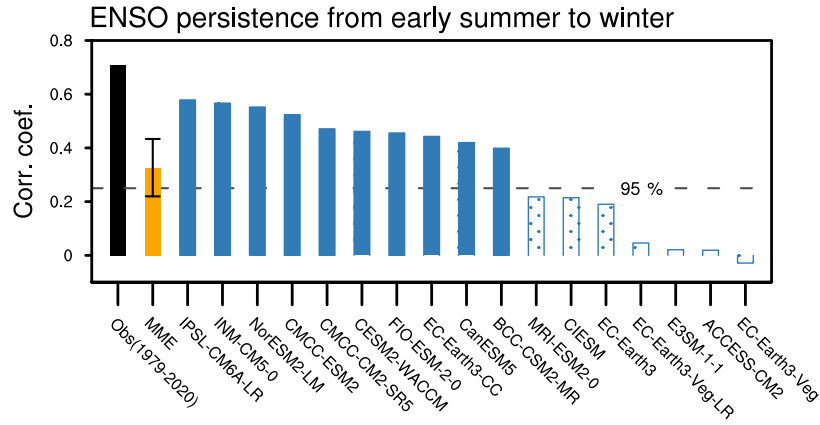


Figure S9. Correlation coefficient of the boreal winter Niño3.4 index with the preceding April-to-June averaged Niño3.4 index for 20 CMIP6 models correctly simulating seasonal synchronization behaviors of both Pacific El Niño and Atlantic Niño. The models are ranked by the correlation coefficients in a descending order. The error bar for the multi-model ensemble (MME) mean corresponds to one standard deviation. The observed value is shown for reference. The dashed line represents the 95% confidence levels.

Table S1. Selected El Niño/La Niña and Atlantic Niño/Atlantic Niña events

Events	Years
El Niño	1982, 1986, 1987, 1991, 1994, 1997, 2002, 2006, 2009, 2015, 2018, 2019
La Niña	1983, 1984, 1988, 1995, 1998, 1999, 2005, 2007, 2010, 2011, 2016, 2017
Atlantic Niño	1981, 1984, 1987, 1988, 1991, 1995, 1996, 1988, 1999, 2003, 2008, 2010, 2016
Atlantic Niña	1982, 1983, 1986, 1990, 1992, 1994, 1997, 2000, 2004, 2005, 2009, 2012, 2015, 2019

Table S2. Extended historical simulations with SSP5-8.5 scenarios from 30 CMIP6 models.

Models	Institution, Country
ACCESS-CM2	CSIRO-ARCCSS, Australia
ACCESS-ESM1-5	CSIRO-ARCCSS, Australia
BCC-CSM2-MR	BCC, China
CAMS-CSM1-0	CAMS, China
CAS-ESM2-0	CAS, China
CanESM5	CCCma, Canada
CESM2-WACCM	NCAR, USA
CIESM	THU, China
CMCC-CM2-SR5	CMCC, Italy
CMCC-ESM2	CMCC, Italy
E3SM-1-1	E3SM-Project
E3SM-1-1-ECA	E3SM-Project
EC-Earth3	EC-Earth-Consortium
EC-Earth3-CC	EC-Earth-Consortium
EC-Earth3-Veg	EC-Earth-Consortium
EC-Earth3-Veg-LR	EC-Earth-Consortium
FIO-ESM-2-0	FIO-QLNM, China
FGOALS-f3-L	CAS, China
FGOALS-g3	CAS, China
GFDL-CM4	NOAA-GFDL, USA
GFDL-ESM4	NOAA-GFDL, USA
INM-CM4-8	INM, Russia
INM-CM5-0	INM, Russia
IPSL-CM6A-LR	IPSL, France
KACE-1-0-G	NIMS-KMA,
MIROC6	MIROC, Japan
MPI-ESM1-2-HR	MPI-M, Germany
MPI-ESM1-2-LR	MPI-M, Germany
MRI-ESM2-0	MRI, Japan
NESM3	NUIST, China
NorESM2-LM	NCC, Norway
NorESM2-MM	NCC, Norway

Table S3. Definitions and values of recharge oscillator model parameters for Eq. (3-8)

Parameter	Estimated value (unit: month ⁻¹)	Definition
ω_a	$2\pi/12$	Angular frequency of annual cycle
ω_s	$2\pi/6$	Angular frequency of semi-annual cycle
R_0	-0.23	Annual mean of R
R_a	-0.070	Annual cycle of R
φ_{R_a}	-0.62	Phase shift of annual cycle modulation
γ_0	0.12	Annual mean of γ
γ_a	-0.060	Annual cycle of γ
φ_{γ_a}	0.65	Phase shift of annual cycle modulation
ε_0	-0.055	Annual mean of ε
ε_a	0.18	Annual cycle of ε
φ_{ε_a}	1.1	Phase shift of annual cycle modulation
λ_0	-0.26	Annual mean of λ
λ_a	-0.15	Annual cycle of λ
φ_{λ_a}	-0.067	Phase shift of annual cycle modulation
α_0	-0.18	Annual mean of α
α_a	-0.063	Annual cycle modulation of α
φ_{α_a}	-0.96	Phase shift of annual cycle modulation
β_0	-0.025	Annual mean of β
β_a	0.017	Annual cycle modulation of β
φ_{β_a}	-0.37	Phase shift of annual cycle modulation